



Experimental Study on the Damage Evolution of Brittle Rock Under Triaxial Confinement with Full Circumferential Strain Control

Thomas Bruning¹ · Murat Karakus¹ · Giang D. Nguyen¹ · David Goodchild²

Received: 19 November 2017 / Accepted: 20 June 2018 / Published online: 30 June 2018
© Springer-Verlag GmbH Austria, part of Springer Nature 2018

Abstract

The identification of crack stress thresholds and damage evolution from circumferential strain control triaxial tests are presented in this paper. As underground excavations become deeper to exploit mineral resources or construct civil projects, it has become increasingly important to determine the full stress–strain and damage evolution behaviours of brittle rock. Therefore, post-peak reaction of Class II rock or ‘snap-back’ behaviour must be captured to show the response of the material under self-sustaining failure. To investigate this, a series of triaxial compression tests were carried out for a granite sourced from over 1000 m depth. The tests were controlled using the feedback of lateral strain gauges attached to the Hoek cell membrane, to allow for constant, slow dilation of the specimen. The test results were then input to existing methods along with two new techniques, to identify the crack stress thresholds of crack closure, crack initiation and damage. It was found that although the crack closure threshold is comparable for axial and lateral control testing, the crack initiation and damage thresholds are significantly higher for the tests conducted in this study compared to most existing research. This result highlights the importance of the circumferential strain control method in triaxial tests when determining the post-peak behaviour and damage evolution of brittle rock. This was made easier with the strain gauged membrane proposed in this study, which provides reliable measurements throughout the duration of rock testing. Therefore, full stress–strain and damage evolution data can be obtained for use in damage–plasticity constitutive models.

Keywords Crack stress thresholds · Damage evolution · Acoustic emission energy · Circumferential strain control · Triaxial tests · Granite

List of Symbols

| | | | |
|------------------|--|-------------------|-----------------------------------|
| E | Elastic modulus | σ_y | Initial yield stress |
| ν | Poisson’s ratio | σ_p | Peak failure stress |
| σ_{UCS} | Uniaxial compressive strength (UCS) | σ_r | Residual stress |
| σ_1 | Axial stress (major principal stress) | ϵ_v^{in} | Inelastic volumetric strain |
| σ_3 | Lateral stress (minor principal stress) | ϵ_s^{in} | Inelastic shear strain |
| ϵ_1 | Axial strain (major principal strain) | p | Hydrostatic stress |
| ϵ_3 | Lateral strain (minor principal strain) | q | Deviatoric stress |
| ϵ_v | Total volumetric strain | K | Bulk modulus |
| ϵ_s | Total shear strain | G | Shear modulus |
| D | Damage variable | σ_{cc} | Crack closure stress threshold |
| Ω | Accumulated acoustic emission energy | σ_{ci} | Crack initiation stress threshold |
| Ω_{total} | Total accumulated acoustic emission energy | σ_{cd} | Crack damage stress threshold |

✉ Thomas Bruning
thomas.bruning@adelaide.edu.au

¹ School of Civil, Environmental and Mining Engineering,
The University of Adelaide, Adelaide, SA, Australia

² OZ Minerals, Level 1, 162 Greenhill Rd, Parkside, SA 5063,
Australia

1 Introduction

Most of the deep mining and civil engineering related underground structures are more commonly being excavated in hard, brittle rock masses. As such it has become increasingly important to better understand the damage evolution

and post-peak behaviour of a rock mass under compressive loading. Numerous studies have concluded that the predominant failure mechanisms for rock are the initiation, propagation and coalescence of micro and macro cracks formed by the redistribution of stresses during or after an excavation (Fredrich and Wong 1986; Martin and Chandler 1994; Oda et al. 2002; Wong 1982). Aside from the direct imaging of microcracks using X-Ray or CT tomography (Fonseka et al. 1985; Tapponnier and Brace 1976; Wong 1982), the most appropriate method for damage assessment is the use of elastic waves emitted during microcrack generation and propagation. The acoustic emission (AE) phenomenon is created by local deformation at the micro scale. At this scale, rock experiences small fracturing events which correspond to the instantaneous release of elastic strain energy in the form of elastic waves. The monitoring of these waves throughout a rock test can give a direct measure of the damage state of the material relative to its original structure (Cox and Meredith 1993; Lockner 1993; Zhang et al. 2015; Zong et al. 2016). This method has also been used for rockburst risk assessment (Ma et al. 2015; Tang et al. 2010) and roof fall prediction (Butt et al. 2000).

An alternative to the acoustic emission method is the identification of stress related damage thresholds. This method, as shown in Fig. 1, characterises the evolution of cracking or damage into several thresholds, typically, crack closure (σ_{cc}), crack initiation (σ_{ci}) and crack damage (σ_{cd}).

The crack closure threshold, σ_{cc} , refers to the point in the test where all pre-existing microcracks in the material have been closed due to compression of the specimen. This threshold is identified when the stress–strain curve becomes linear or when the inelastic volumetric strain plateaus indicating no further, permanent compaction. After crack closure, a material will behave elastically until the onset of dilation caused by the initiation of microcracks. The crack initiation threshold, σ_{ci} , is therefore calculated as the onset of inelastic deformation (dilation) after the linear elastic loading phase. The cracking which initiates at this stage of loading is considered to be stable as it requires an increase in load to induce further dilation and cracking in the specimen. Finally, the point at which a reversal of total volumetric strain occurs is referred to as the crack damage threshold, σ_{cd} . This assumes that the switch from compaction to dilation behaviour is the result of microcracks in the specimen starting to open and coalesce and damage evolution becomes unstable (Bieniawski 1967a, b; Eberhardt et al. 1999, 1998; Martin 1993; Martin and Chandler 1994; Wawersik and Fairhurst 1970).

The calculation of these thresholds, first proposed by Bieniawski (1967a), were then expanded by Eberhardt et al. (1998) to include the change in axial stiffness as another measure of the crack closure and initiation thresholds. It can be seen from Fig. 2 that as the average axial stiffness plateaus, signifying the beginning of linear elasticity, crack closure is assumed to be complete. Following this, the departure

Fig. 1 Stages of crack development in rock during uniaxial compressive test. Modified from Eberhardt et al. (1998)

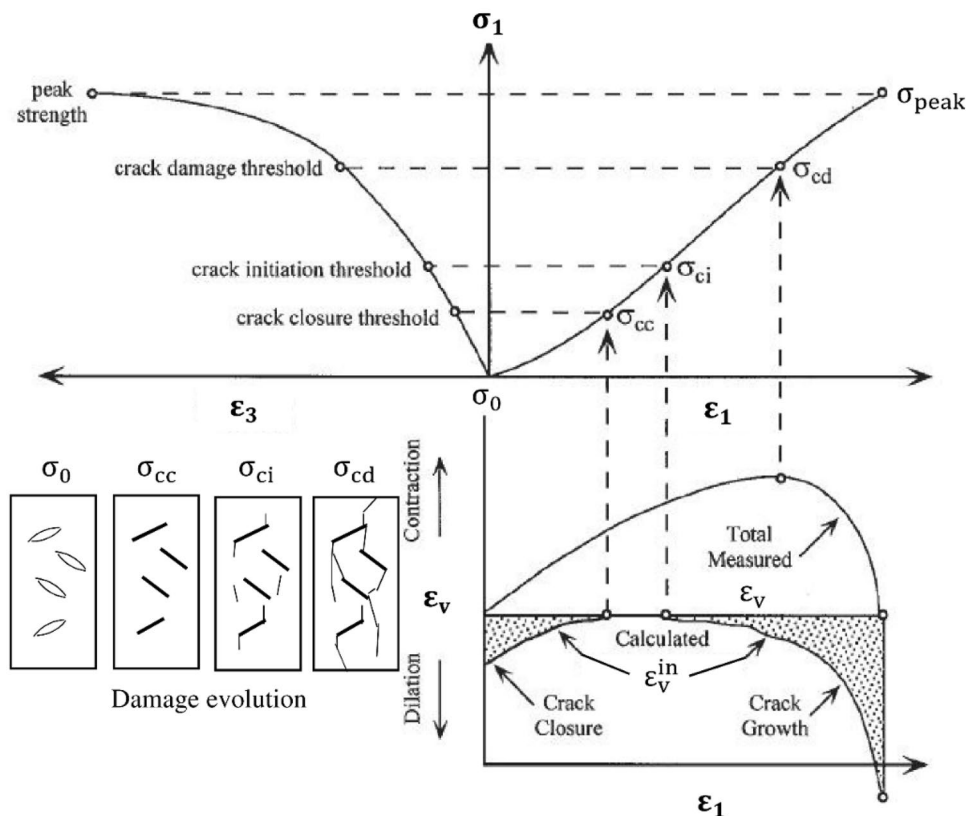
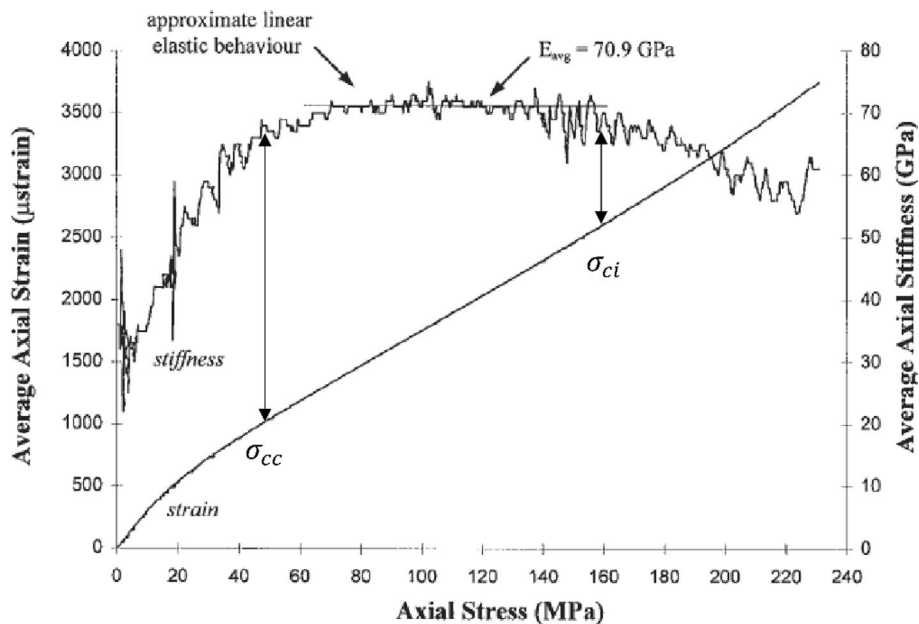


Fig. 2 Example of crack closure and initiation thresholds derived from average axial stiffness by Eberhardt et al. (1998)



of the average axial stiffness from this plateau indicates the onset of microcrack growth and hence crack initiation.

Further developments in the field lead to the formation of objective methods to determine the damage thresholds of a rock. Focussing on the lateral strain measure, Nicksiar and Martin (2012) developed the Lateral Strain Response (LSR) method shown in Fig. 3. This method uses the point of maximum volumetric strain as a reference and determines the point of maximum lateral strain difference which signifies the start of crack initiation (Nicksiar and Martin 2012). Another similar objective method was proposed by Zhao et al. (2015) which used the proposed cumulative AE hit method to predict the crack initiation threshold.

The strain, stiffness and acoustic emission methods have been widely used for various rock types and as such, extensive data have been accumulated. Table 1 is a compilation of a variety of hard rock studies and subsequent

values for damage thresholds where the confinement level of each study is shown as σ_3 . It is clear from Table 1 that although there has been numerous tests conducted on hard rocks that show the thresholds as being consistent, they all share the same loading methodology or similar. Studies that do include the effects of circumferential control are few and only uniaxial in nature (Nicksiar and Martin 2012; Zhao et al. 2015). There are no current studies that report the calculation of damage thresholds specifically for circumferentially controlled, triaxial tests and overall, there is limited information on the effects of confinement on damage threshold values for hard igneous rock (see Fig. 4).

The axial control of a compression test is traditionally achieved by setting a constant displacement or load throughout the duration of a test. This is often sufficient for soft rocks; however, it has been pointed out by Fairhurst and Hudson (1999) to be insufficient for brittle rock, as it is

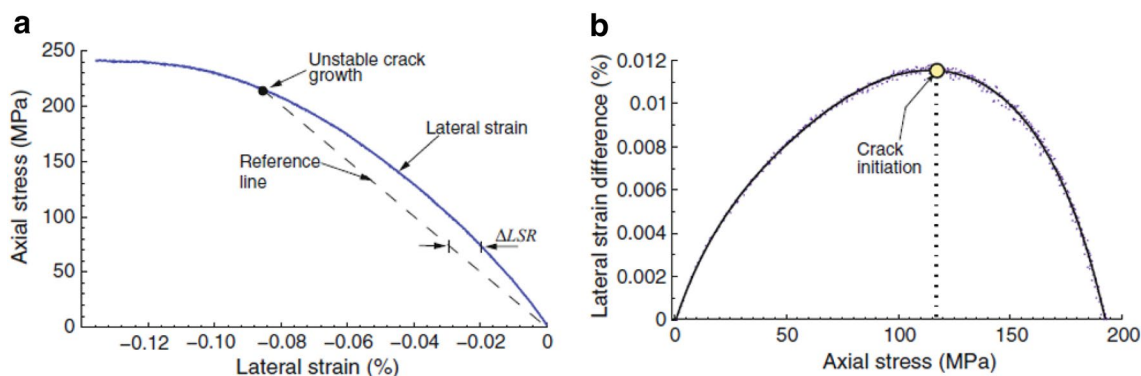
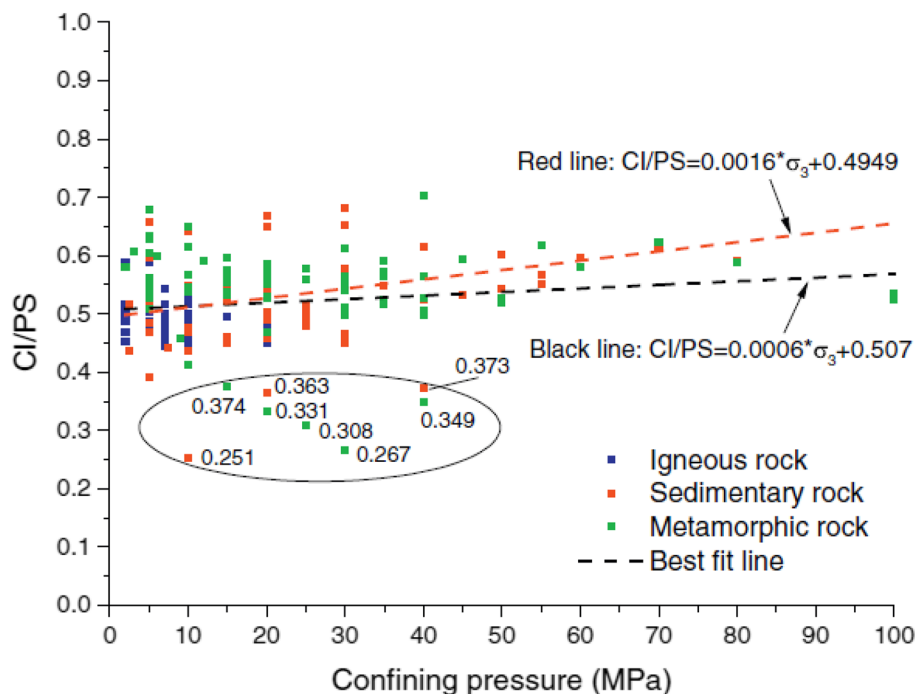


Fig. 3 Lateral strain response method proposed by Nicksiar and Martin (2012)

Table 1 Experimental damage threshold values for hard rock

| Rock | σ_3 (MPa) | $\frac{\sigma_{cc}}{\sigma_p}$ | $\frac{\sigma_{ci}}{\sigma_p}$ | $\frac{\sigma_{cd}}{\sigma_p}$ | Test control | References |
|----------|------------------|--------------------------------|--------------------------------|--------------------------------|-----------------|-----------------------------|
| Diorite | 0 | – | 0.51 | 0.90 | Axial load | Hidalgo and Nordlund (2013) |
| Diorite | 0 | – | 0.49 | – | Circumferential | Nicksiar and Martin (2012) |
| Dolomite | 0–25 | – | 0.71 | 0.90 | Axial disp. | Hatzor and Palchik (1997) |
| Gabbro | 0 | – | 0.58 | 0.80 | Axial load | Hidalgo and Nordlund (2013) |
| Granite | 0 | 0.23 | 0.39 | 0.76 | Axial disp. | Eberhardt et al. (1998) |
| Granite | 0–60 | – | 0.48 | 0.61 | Axial disp. | Hoek and Martin (2014) |
| Granite | 0 | – | 0.48 | 0.60 | Axial disp. | Ghazvinian et al. (2015) |
| Granite | 0–20 | 0.10 | 0.40 | 0.84 | Axial disp. | Chang and Lee (2004) |
| Granite | 0 | – | 0.39 | 0.75 | Axial disp. | Eberhardt et al. (1999) |
| Granite | 41 | – | 0.40 | 0.84 | Axial disp. | Katz and Reches (2004) |
| Granite | 0 | – | 0.36 | 0.80 | Axial disp. | Martin (1993) |
| Granite | 4.9 | – | 0.40 | 0.71 | Axial disp. | Heo et al. (2001) |
| Granite | 0 | 0.39 | 0.51 | 0.71 | Axial disp. | Kim et al. (2015) |
| Granite | 0 | – | 0.52 | 0.81 | Axial load | Hidalgo and Nordlund (2013) |
| Granite | 0 | – | 0.43 | 0.76 | Axial load | Hidalgo and Nordlund (2013) |
| Granite | 0–40 | – | 0.48 | 0.80 | Unknown | Zhao et al. (2013) |
| Mixed | 0 | – | 0.48 | – | Circumferential | Zhao et al. (2015) |

Fig. 4 Compilation of calculated crack initiation thresholds for rock (where CI/PS is the ratio of crack initiation and peak stresses) (Wen et al. 2018)



usually impossible to obtain the full stress–strain response of a specimen under varying confinement due to self-sustaining failure.

It was first demonstrated by Wawersik (1968) that brittle rock tends to exhibit ‘snap-back’ behaviour during compressional loading at low confinements. This led to the classification of post-peak behaviour of rocks into Class I and II. Class I behaviour is when a rock is soft and to induce further strength reduction, increased deformation must be applied

to the specimen. Class II on the other hand is very brittle behaviour where the strength reduction is self-sustaining due to the built-up elastic strain energy in a specimen. Class II behaviour is seen commonly in brittle rocks (Labuz and Biolzi 1991; Wawersik 1968).

Initial attempts to obtain the full stress–strain behaviour of a rock during compression concentrated on the stiffness of the loading system (Hudson et al. 1970, 1972; Wawersik 1968; Wawersik and Brace 1971; Wawersik and Fairhurst

1970), however, more recently it is thought that by controlling the application of load through a feedback loop of circumferential strain, the correct behaviour of each test can be obtained (Fairhurst and Hudson 1999). Hence, it stands to reason that if the full failure process of a brittle rock cannot be captured by a constant axial loading methodology, then the damage thresholds could also prove to be reliant on the loading method.

As can be seen in Fig. 5, the surplus stored elastic strain energy in a Class II rock allows for self-sustaining failure. Therefore, it stands to reason that if energy is constantly applied during a test, the cracking of a rock cannot be controlled past the very early stages of failure. This could correspond to under-estimation of the crack initiation and damage thresholds, making it difficult to determine the onset of damage-plasticity behaviour for brittle rock.

This paper investigates the damage thresholds and overall evolution of circumferentially controlled triaxial compression tests of granite. This method captures the full stress–strain behaviour of brittle rock, and therefore, the damage thresholds and ‘snap-back’ behaviour can be obtained. Furthermore, multiple confinements were tested to uncover any relationships it may have to damage evolution. Although it is widely accepted that the damage thresholds of a rock are material parameters, this study aims to provide evidence that there is some reliance on the control method used to conduct a test. Hence, we will attempt to provide a basis for understanding the damage evolution in close comparison to full compressive stress–strain responses. This should enable more accurate analysis using damage-plasticity models such as those proposed by Salari et al. (2004), Unteregger et al. (2015) and Bruning et al. (2016). This, in

turn, would lead to reliable numerical modelling of rock behaviour under high confining pressures.

2 Experimental Procedure

2.1 Sample Preparation and Loading Method

The rock used in this experimental investigation is a granite sourced from a borehole located in South Australia at a depth of 1020–1035 m. It is generally observed as coarse grained, massive granite with weak to moderate alteration, occasionally with weak gneissic foliation. This is a brittle rock with grain size ranging from 0.5 to 3 mm and a density of 2730 kg/m³. The mineral composition of the granite almost exclusively consists of potassium feldspar, quartz and chlorite. The alteration materials found in the samples are predominantly red earthy hematite and minor chlorite and occasionally display veins and stringers of dark-grey hematite, red earthy hematite, chlorite, quartz and carbonate.

Samples were prepared in accordance with the ISRM suggested method for triaxial compression testing (ISRM 2007). As uniaxial compressive strength (UCS) test results of the rock type showed an average strength of $\sigma_{\text{UCS}} = 158$ MPa, the 63-mm-diameter drill core was sub-cored to 42 mm diameter and cut to 100 mm in length to allow for higher confining pressures during triaxial testing. The ends were ground and polished to allow for consistent contact with the test platens.

The loading method used in this study was based on the technique outlined in the ISRM method for obtaining the complete stress–strain curve in a compressive test (Fairhurst and Hudson 1999). As stated in the standard, the specimen was loaded axially such that the growth of circumferential strain ($\Delta\varepsilon_3$) was constant at 1×10^{-5} mm/mm/s. To begin each test, the rock specimen was loaded into the triaxial cell and confining pressure was applied by the cell and loading frame up to the desired isotropic loading condition. Then as lateral pressure remained constant, axial loading was applied using the circumferential control method. This method differed from the standard in that there was no initial axial displacement or load control of the specimen.

To ensure there were no strength losses due to the proposed loading, UCS tests were conducted using this slightly adjusted method and the exact method outlined in the ISRM standard (Table 2). It was found that both methods returned approximately the same average and range for peak stress. Furthermore, the LSR method was used to calculate the crack initiation and damage thresholds for the tests. It can be seen in Table 2 that both methods return acceptable values for the thresholds based on previous research (Table 1; Fig. 4). Therefore, the method was deemed suitable for application to triaxial testing in

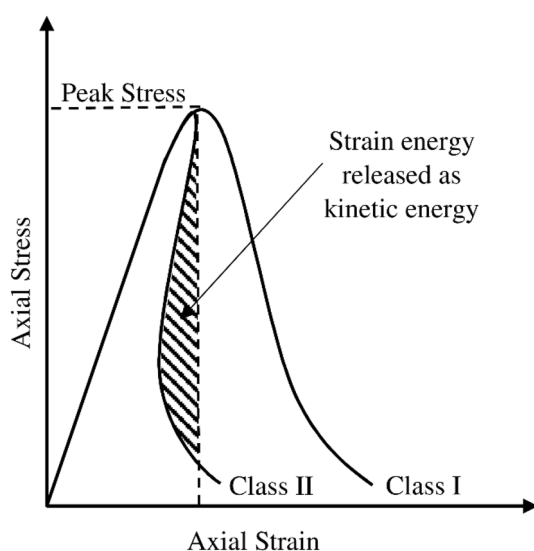


Fig. 5 Energy difference between Class I and II rocks

Table 2 UCS results for conventional (ISRM) and full circumferential strain control (FCC) loading methods

| Sample ID | Loading method | UCS (MPa) | $\frac{\sigma_{ei}}{\sigma_p}$ | $\frac{\sigma_{ed}}{\sigma_p}$ | Average UCS (MPa) |
|-----------|----------------|-----------|--------------------------------|--------------------------------|-------------------|
| UCS-1 | ISRM | 188 | 0.55 | 0.92 | 159 |
| UCS-2 | ISRM | 171 | 0.52 | 0.91 | |
| UCS-3 | ISRM | 127 | 0.53 | 0.93 | |
| UCS-4 | FCC | 168 | 0.55 | 0.93 | 156 |
| UCS-5 | FCC | 124 | 0.53 | 0.90 | |
| UCS-6 | FCC | 175 | 0.49 | 0.90 | |

this study. The overall goal of this adjusted method was to investigate the effect circumferential strain control has on a test during the pre-peak response. This also largely avoided the situation of complete brittle failure of the material observed in axial control tests due to the constant application of pressure in the initial stages of loading which causes damage accumulation. This in turn allowed the capturing of full Class II behaviour. This loading scenario was able to provide the maximum level of control of the failure process of hard rock and to enable accurate and precise measurement of the characteristic damage evolution of the material without the effect of the loading rate. This method has also been adopted in industry but at much faster lateral strain rates. These are normally calibrated to reflect an equivalent axial load control (Eloranta 2004; Jacobsson 2004a, b).

In this study, compressive stresses and strains are defined as positive. The principal stresses are in the axial (σ_1) and radial (σ_3) directions in triaxial space. As explained, the axial (ϵ_1) and radial (ϵ_3) strains are directly measured from the tests and used to define volumetric and shear strains given by $\epsilon_v = \epsilon_1 + 2\epsilon_3$ and $\epsilon_s = \frac{2(\epsilon_1 - \epsilon_3)}{3}$, respectively (Puzrin 2012).

2.2 Triaxial Compression Tests

The testing frame used to carry out triaxial compression tests was an INSTRON 1282 with an axial load capacity of 1000 kN. Specimen confinement was achieved using a Hoek cell with capacity up to 65 MPa. Linear variable differential transformers (LVDTs) were used to measure the axial strain and all data acquisitions were done using a National Instruments cDAQ module. To measure the circumferential strain for each test, a Hoek cell membrane was fitted with four strain gauges internally within the cell. This was achieved by fitting a high pressure wire feed through connector to the cell. Each gauge was attached immediately alongside one another around the centre of the liner and connected to a Wheatstone bridge to provide the input for the control circuit. This then averaged the signal received by each gauge and thus provided accurate measurements of the circumferential strain of each specimen. This signal was then input into the Instron Labtronic 8800 control unit which controlled the test based on circumferential strain rate. The wiring and setup for this method is shown in Fig. 6.

To ensure this method was accurate, strain gauges were also attached directly to the specimen for low confinement tests (10 and 20 MPa) and the strain response was compared. Figure 7 shows the comparison between the two lateral strain measurement methods for tests where the specimen gauges survived until post-peak loading. It is clear that no significant resolution or behaviour was lost using the gauged membrane method. The small offset in lateral strain magnitudes was a consequence of averaging four strain gauges around the entire outside diameter of the membrane as opposed to the averaging of two attached to the specimen. Additionally, strain gauges attached to the specimen were commonly broken at early stages in the test (elastic material loading). This can occur even at low confining pressures. This resulted in the loss of the ability to average gauges around the specimen, and therefore, lateral strain output would become location

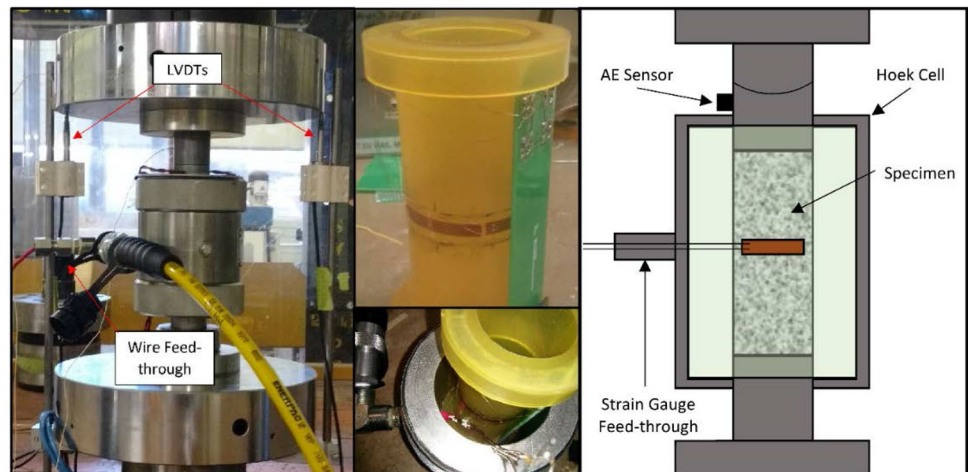
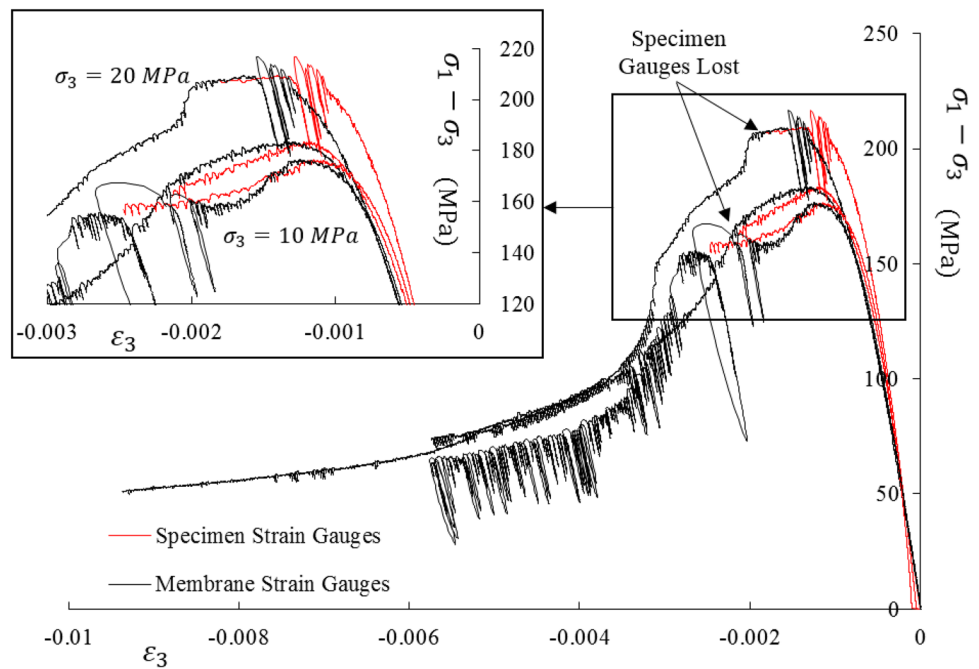
Fig. 6 Strain gauged membrane and test set-up

Fig. 7 Comparison of lateral strain gauge responses attached to membrane and rock



dependent. It can also be seen that when larger radial strains were reached during post-peak loading, gauges attached directly to the specimen were lost due to excessive pressure and deformation. Therefore, as the membrane gauges survived the entire experiment and could reduce local variance due to the averaging of four gauges, they were used for all tests for accurate measurement of lateral strains and for circumferential control.

2.3 Acoustic Emission Monitoring

Throughout testing the acoustic emissions of each specimen were recorded by placing sensors on the loading piston and spherical seat directly above the specimen. The sensor on the loading piston was to enable the identification and filtering of any mechanical noise due to the loading frame. The acoustic signals were captured using miniature PICO sensors and were passed through a pre-amplifier set to 60dB of gain (Type 2/4/6). Express-8 data acquisition card was used and sampling rate was set to a 2 MSPS (mega samples per second). The signal then was processed using the MISTRAS AWin software. The lower threshold value for mechanical and ambient noise was set 45 dB. This was established by setting a low threshold (20 dB) then increasing until the loading frame noise was no longer registering during acquisition. This is a widely adopted method to calibrate this threshold before each test as the environmental noise for each laboratory is different. To ensure the acoustic emissions could be compared to certain loading scenarios, the recording for stress–strain and acoustic emissions signals was simultaneously started for each test. To quantify the

damage from acoustic emissions the following relationship was implemented:

$$D = \frac{\Omega}{\Omega_{total}}, \tag{1}$$

where Ω is the accumulated acoustic emission energy at a certain time of the test, Ω_{total} is the total acoustic energy over the whole duration and D is the damage variable. It is also important to note that $0 \leq \Omega \leq \Omega_{total}$ and $0 \leq D \leq 1$, where 0 represents the initial undamaged state of the material and 1 is the point of final frictional failure. The definition of damage using AE energy has been discussed in the literature by previous researchers (Akdag et al. 2018; Grosse and Ohtsu 2008; Ji et al. 2014; Kim et al. 2015). It is concluded by these studies that the energy associated with AE response is more representative of the extent of microcracking in rock than the recorded hits. Therefore, the cumulative energy approach given in Eq. 1 was used to quantify the relative damage levels in this study.

3 Experimental Results

Triaxial compression tests were conducted on the prepared specimens over the confining pressure range of 10–60 MPa. Results for all successful tests are presented in Table 2 where σ_3 is the confinement of the test, σ_y , σ_p and σ_r are the initial yield, peak and residual strengths, respectively, and Young’s Modulus, E and Poisson’s ratio, ν of each specimen. In this sense, initial yield is determined as the point the stress–strain curve departs elastic linearity and the residual

strength is the plateau of the post-peak reaction. As some tests produced very large data sets, the residual portions of some individual experiments have been cropped to ensure the figure is clear. Despite the careful control strategy in place, some samples were still lost to brittle failure due to existing discontinuities. This mobilised the failure too fast for some specimens (TX10-1, TX20-4, TX30-3 and TX40-2) during triaxial testing. These results were excluded from the study to avoid inconsistency.

The full stress–strain response for each test is given in Fig. 8.

It can be seen from Fig. 8 that at confinements below 40 MPa the predominant failure mode is Class II. However, beyond this confinement it is observed that the granite tested seems to transition to more instances of Class I behaviour. It is believed by these researchers that as confinement level increases, there is more opposition to self-sustaining failure. This means that for the rock to continue to yield, more energy must be added to the system via the continued application of axial load. Conversely, at low confinements, the

rock stores adequate energy during the pre-peak phase of loading to continue to fail under little to no added external work. It is interesting to note that at 40 MPa confinement for this rock, both Class I and II behaviours were recorded. A zoomed-in picture of the 40 MPa tests is given in Fig. 9.

To provide a full characteristic dataset for the rock, the axial stiffness and Poisson's ratio were plotted for each confining pressure (Fig. 10). It was found that stiffness increased with confining pressure and Poisson's ratio is constant throughout the confining pressure range.

3.1 Damage Evolution

This study has already postulated that the cumulative acoustic emission energy relates to damage using Eq. 1, and therefore, it was possible to gather information about the damage evolution of the material under different levels of confinement. As such, the damage variable from the AE response captured in each test was compared with axial strain. It is

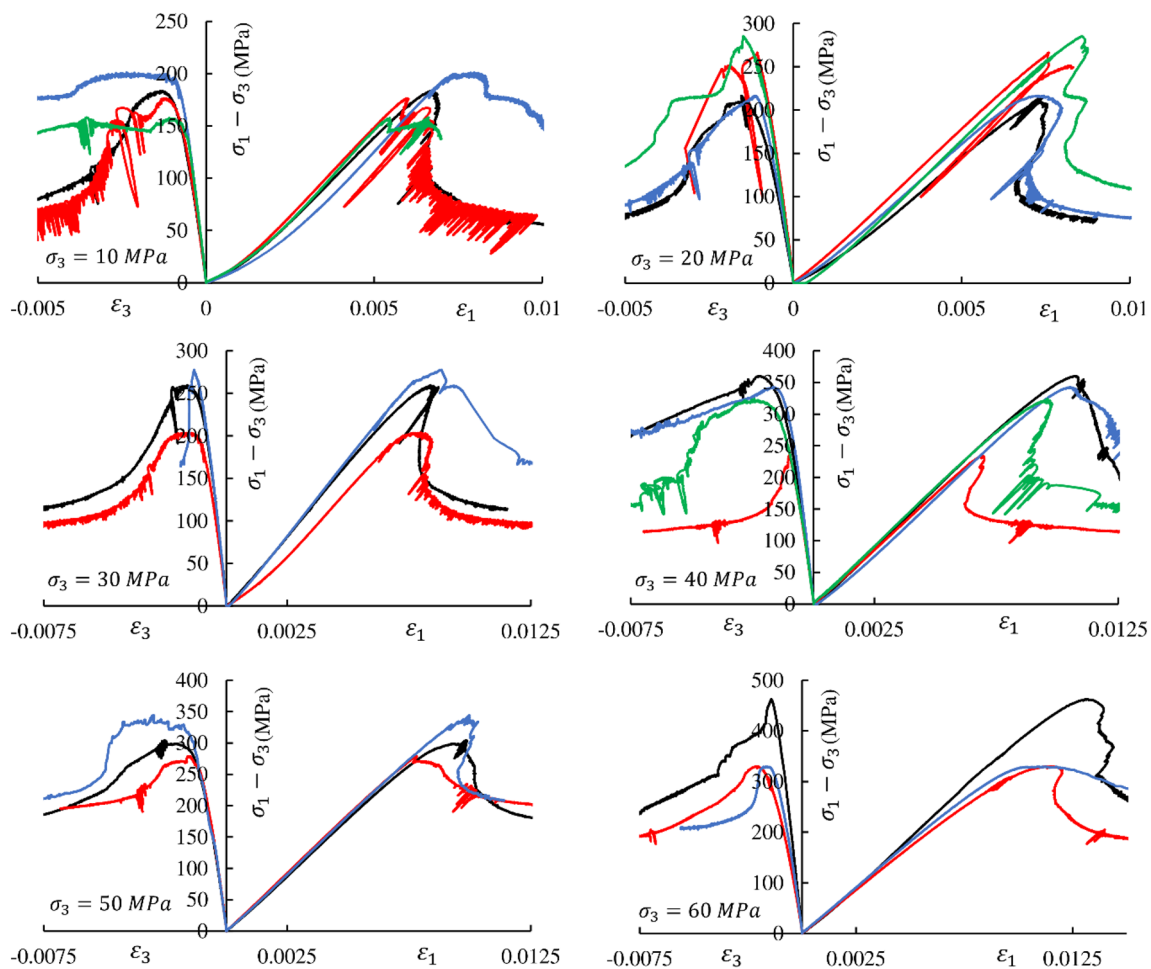


Fig. 8 Test data for each confinement level (10–60 MPa)

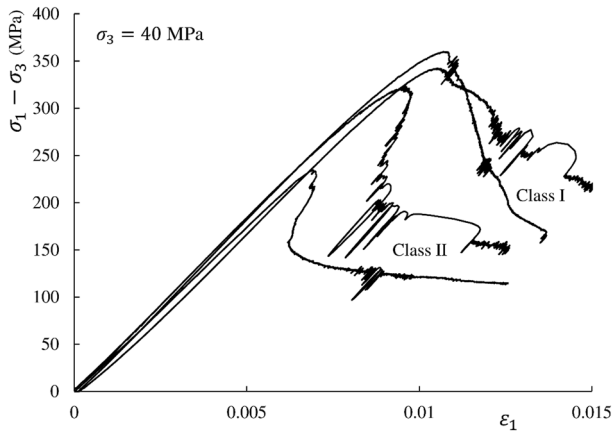


Fig. 9 Class I and II behaviours of granite at 40 MPa confinement

important to note that all analyses in this section were undertaken on individual tests and no averaging of data over similar confinement pressures was undertaken. This ensured that the AE response was coupled with the stress–strain results correctly for each test. Examples of an individual acoustic response for each confinement are presented in Fig. 11 and it can be seen that as lateral pressure increases the emissions occur more gradually with increasing axial strain. This corresponds to the damage evolution process becoming slower due to the increasing degree of opposing stress imparted by confinement. In other words, the hardening and more gradual softening behaviour of a rock under high confinement corresponds to the rate of microcrack initiation, propagation and coalescence competing against the consolidation effect of lateral pressure.

Furthermore, as rock undergoes compressive deformation, microcrack development increases, which is evident by the increased rate of acoustic emission signals. It has also been observed in experiments that as the number of microcracks (damage) increases in a material during testing, the stiffness of the rock decreases (Chen et al. 2014, 2015; Eberhardt et al. 1999). Therefore, to describe this overall behaviour, the scalar

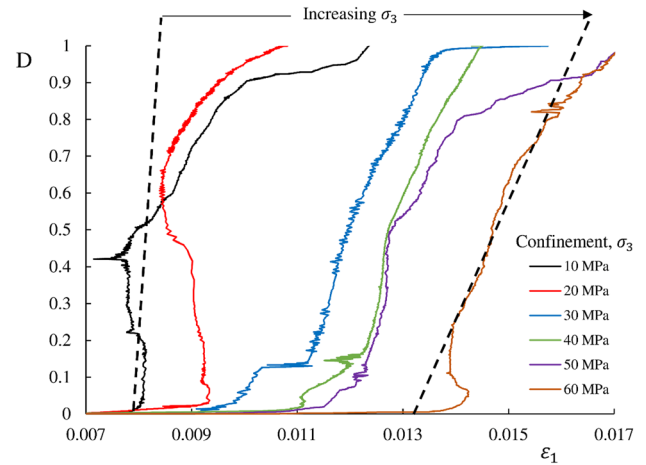


Fig. 11 Effect of confinement pressure on damage evolution based on AE response

damage parameter outlined by Eq. 1 was used in the damage mechanics framework described in the works by Krajcinovic (1996), Lemaitre and Desmorat (2005) and Murakami (2012):

$$p = (1 - D)K(\epsilon_v - \epsilon_v^{in}), \tag{2}$$

$$q = (1 - D)3G(\epsilon_s - \epsilon_s^{in}), \tag{3}$$

where K and G are the elastic bulk and shear moduli, respectively. Therefore, the triaxial volumetric and shear inelastic strains throughout testing are implicitly assumed to take the form:

$$\epsilon_v^{in} = \epsilon_v - \frac{p}{(1 - D)K} = \epsilon_v - \left[\left(\frac{1 - 2\nu}{(1 - D)E} \right) (\sigma_1 + 2\sigma_3) \right], \tag{4}$$

$$\epsilon_s^{in} = \epsilon_s - \frac{q}{(1 - D)3G} = \epsilon_s - \left[\frac{\sigma_1 - \sigma_3}{(1 - D)3G} \right]. \tag{5}$$

It is acknowledged that the damage state defined in the above relationships is assumed to correlate to the acoustic

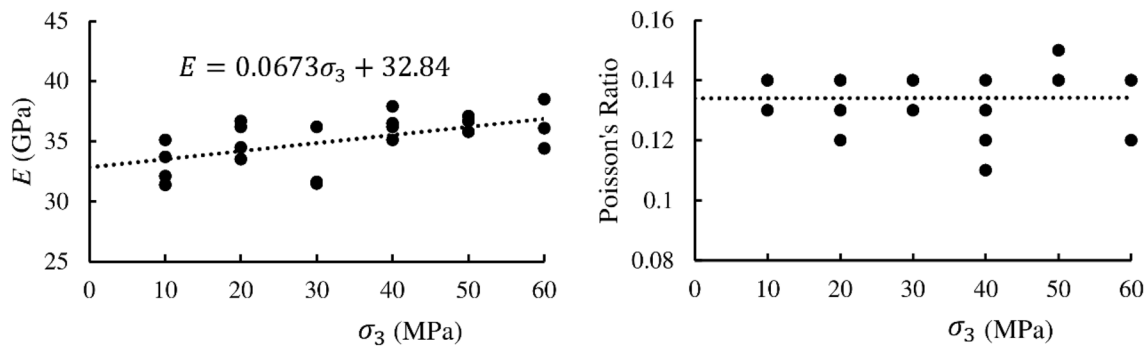


Fig. 10 Elastic constants of each triaxial test (due to data overlap please refer to Table 2 for individual results)

emission definition (Eq. 1) provided in this research. Given the fact that microcrack formation and propagation in rock specimen affects the elastic stiffness, this assumption is reasonable in our opinion and can be used for quantifying the experimental results.

Once the inelastic strains were calculated, they were compared to the damage variable shown in Fig. 12. This revealed for a representative test that as confinement increases, the damage evolution of the material is more gradual over increasing permanent deformation of the material. Data such as this could be used to calibrate or form damage evolution laws for constitutive modelling.

4 Damage Threshold Estimation

This section focuses on the determination of the damage thresholds for the triaxial compression of rock using methods from previous publications as well as the proposed inelastic strain and acoustic emission techniques. To date, limited research has been done to apply these methods to fully circumferential strain controlled, triaxial tests. Therefore, as the true pre- and post-peak behaviours of Class II rocks are not accounted for, differences in the calculated values for thresholds could exist for hard rocks. Additionally, very few studies have dealt with the calculation of these thresholds for confined igneous specimens (Wen et al. 2018). As such it is important to provide a comprehensive study on the calculation of crack damage thresholds for the tests conducted in this research. For the granite specimens tested, the full Class I and II stress–strain responses were successfully recorded. Therefore, the calculation of these thresholds in this section can be compared to the literature results and discussed.

The first method utilised was after Martin (1993). Shown in detail in Fig. 1, the total volumetric strain from each test

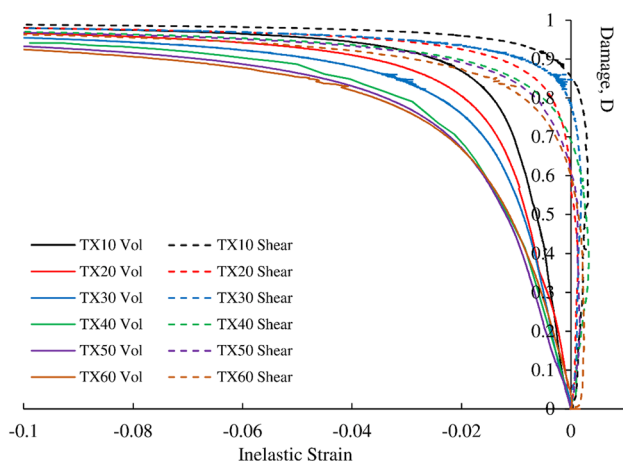


Fig. 12 Damage evolution with inelastic strains (shear and volumetric) at various triaxial (TX) stresses

was plotted and compared to find the crack damage threshold (σ_{cd}). The initial estimates of crack initiation were done using the axial strain method (ASM) proposed by Eberhardt et al. (1998), the lateral strain response (LSR) method Nicksiar and Martin (2012) and the accumulated AE hit method (CAEM) outlined in Zhao et al. (2013). These methods were then used as a baseline for validating the proposed methods in this study.

The damage inelastic strain method (DISM) used in this study was modified from those used widely in the literature (Martin 1993). This was done by comparing the damage state at a certain axial strain increment using Eq. 1 and inputting into the triaxial stress–strain relationships to calculate inelastic volumetric (ϵ_v^{in} , Eq. 4) and shear (ϵ_s^{in} , Eq. 5) strains. The values for inelastic volumetric and shear strains were then graphed against axial strain and cross-referenced with the stress and damage curves to determine the location of crack closure (σ_{cc}) and crack initiation (σ_{ci}). The results are similar in nature to those shown in Fig. 1, however, by including the damage variable in the calculation of the inelastic strains, the dependence of crack thresholds on constant elastic parameters highlighted by Eberhardt et al. (1998) could be avoided.

The other proposed technique to determine damage thresholds was the acoustic emission damage method (AEDM). The calculation of a damage variable using acoustic emission energy (Eq. 1) has not been used by many studies (Akdag et al. 2018; Grosse and Ohtsu 2008; Ji et al. 2014; Kim et al. 2015) and only the cumulative hits method has been applied to crack damage thresholds. Therefore, as energy reveals much more about the magnitude of microcracks (and hence provides a more quantifiable measure), it is crucial to calculate the crack damage thresholds using this measurement. It was found that the crack initiation threshold could be estimated by the point where acoustic emission activity begins after the linear elastic phase of loading. Then the crack damage threshold can be calculated as the increase in damage evolution, indicated by a change in slope of the damage vs. axial strain curve due to the acceleration of microcracking and unstable fracture propagation. The calculation of these thresholds using acoustic energy is shown in Fig. 13 for a triaxial test with a confining pressure of 30 MPa conducted in this research.

Once each test was conducted, all of the methods described above were implemented to calculate the crack damage thresholds. Figures 14, 15, 16, 17, 18 and 19 present a typical full dataset for a test at each confinement. As LSR is not plotted against axial strain, these graphs were omitted from the figure. By applying each of the methods and displaying them all together it was possible to compare the result of each method and hence determine the effectiveness of each to determine the crack thresholds. Although only a single test is given in full for each confinement, the

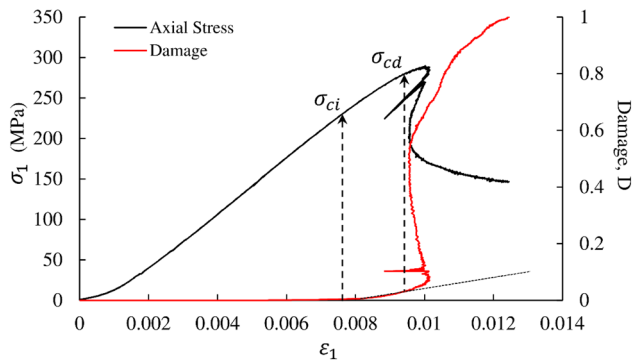


Fig. 13 Determination of damage thresholds from damage parameter/acoustic emissions energy

calculations were done for every sample listed in Table 3. Therefore, further discussion on the crack damage thresholds is based on at least three tests at each confining pressure. Table 4 displays the results of every method along with overall statistics for each test and confinement where SD is standard deviation and CoV is the coefficient of variance.

It can be seen that crack closure is consistently calculated by the inelastic volumetric strain and average axial stiffness methods. However, the step size for the moving point regression technique can affect the location of the plateau for lower confinement tests. Therefore, the more accurate method for determining the crack closure threshold was found to be the modified inelastic volumetric strain curve.

Figures 14, 15, 16, 17, 18 and 19 and Table 4 also show that the crack initiation thresholds show good agreement for all of the prediction methods. Therefore, the onset of damage and hence initial yield of the material can be calculated with confidence from these circumferentially controlled tests. Therefore, due to the correlation between the methods of this initial yield estimation, damage-plasticity numerical models can be calibrated to this stress level and damage evolution studied from the initiation point.

Furthermore, the crack damage threshold was found using total volumetric strain at the onset of dilation and the proposed AE method. These two methods predicted the same value for this threshold, and therefore, it was concluded that sufficient accuracy of the AE emission energy method was achieved. It was also found that the rate of inelastic shear and volumetric strain increased at the calculated point of crack damage. Figure 20 shows the increase in inelastic strains corresponding to the point of maximum total volumetric strain. Therefore, it is concluded that this measure can also be used to predict the crack damage threshold of a circumferentially controlled test.

Once the process of estimation was conducted for each test, the results were compiled and plotted to show the relationship between the thresholds and confinement. Figure 21 graphically displays the proportion of peak stress for each

damage threshold and also shows the standard deviation of the results for each confinement.

5 Discussion

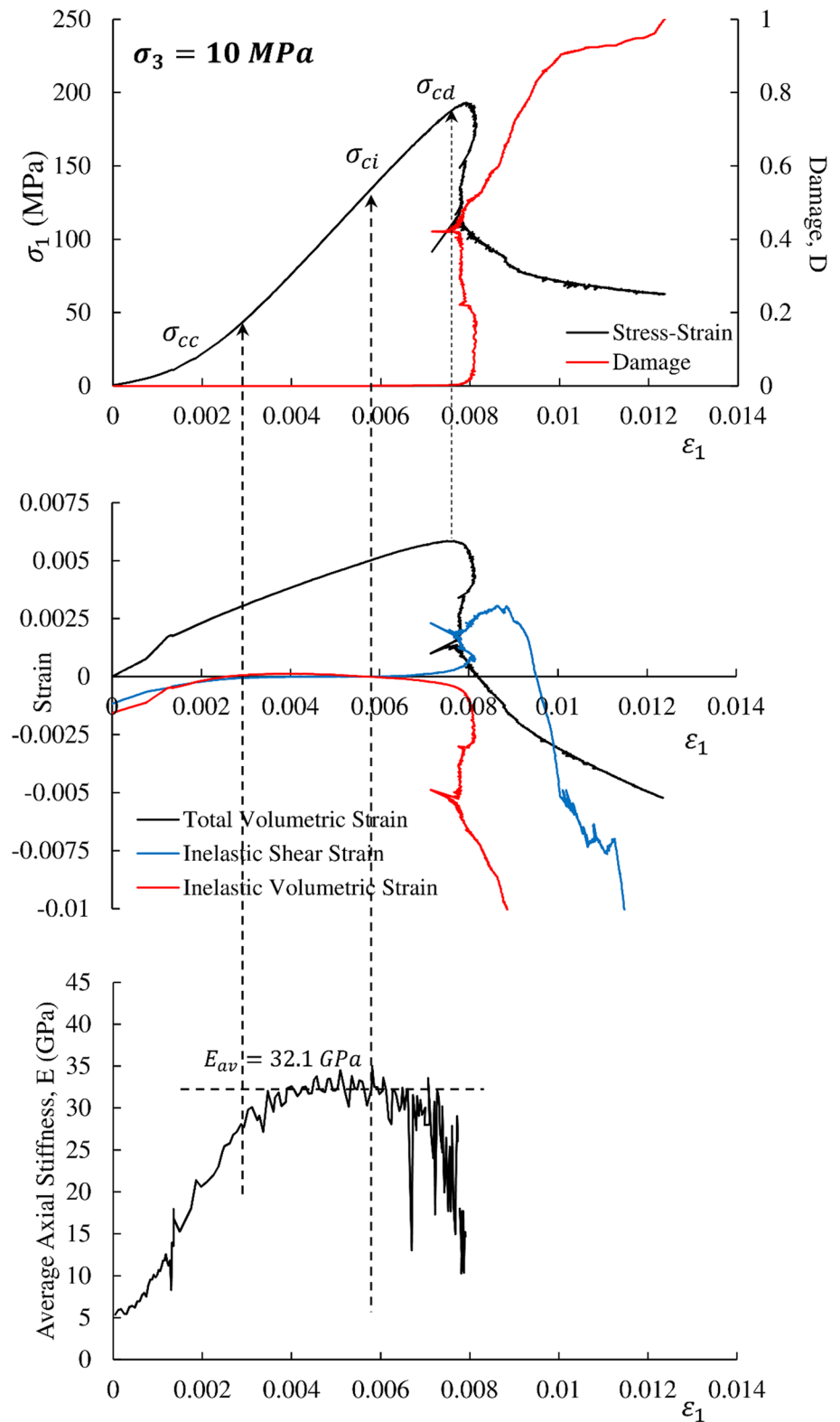
Estimations of damage thresholds in the literature have usually revealed that crack closure occurs at around 20% of peak stress (Eberhardt et al. 1999, 1998). The test results in this study also display that this threshold holds true under the FCC method, however, some variation of test results was also realised. It is postulated to be the result of the different extent and properties of microcracking present in each sample before testing. Therefore, the samples can take variable proportions of peak stress to consolidate and for microcracks to close. The most effective method for measuring the crack closure threshold was found to be the modified inelastic volumetric strain method (Eq. 4) as this coincided much more closely to the stress–strain linearisation than the stiffness method for all confinement levels. This is due to the effect of the range of values employed for the moving point regression technique on the stiffness method.

The crack initiation thresholds calculated in this research were found to be higher than for most other tests found in previous studies. Contrary to the 50–60% of peak stress found for granitic rocks in existing publications (Table 1; Fig. 4), the crack initiation threshold was found to be in the range of 60–70% of peak stress. The contrast is displayed graphically in Fig. 22. Although the thresholds are relatively high, the levels have been recorded in the past by Hatzor and Palchik (1997).

It is also apparent from the FCC tests that as confinement increases, the proportional crack initiation stress increases. Therefore, although the loading control does seem to effect the magnitude of the crack initiation threshold, the overall increasing trend is not affected. This can also be seen in Fig. 22 as the current research displays the same slope as the compiled results for all rocks in Wen et al. (2018). Furthermore, the crack initiation threshold from circumferential control tests could be used as the initial yield point of a material in a plasticity or damage-plasticity constitutive model. This is a more accurate estimate than relying on the deviation of axial stiffness alone as there is obscurity with the estimation of the point at which the Young's modulus decreases enough to identify overall structural weakening of the material. Additionally, as the test is controlled by dilation, it is less likely that there is a sudden failure of the specimen. Therefore, the initial yield of the material can be captured somewhat independent of loading rate.

Another important finding of these tests is the predictor for the crack damage threshold for each test. The results do not match typical results nor behaviours reported in numerous studies on granite or similar rocks under axial pre-peak

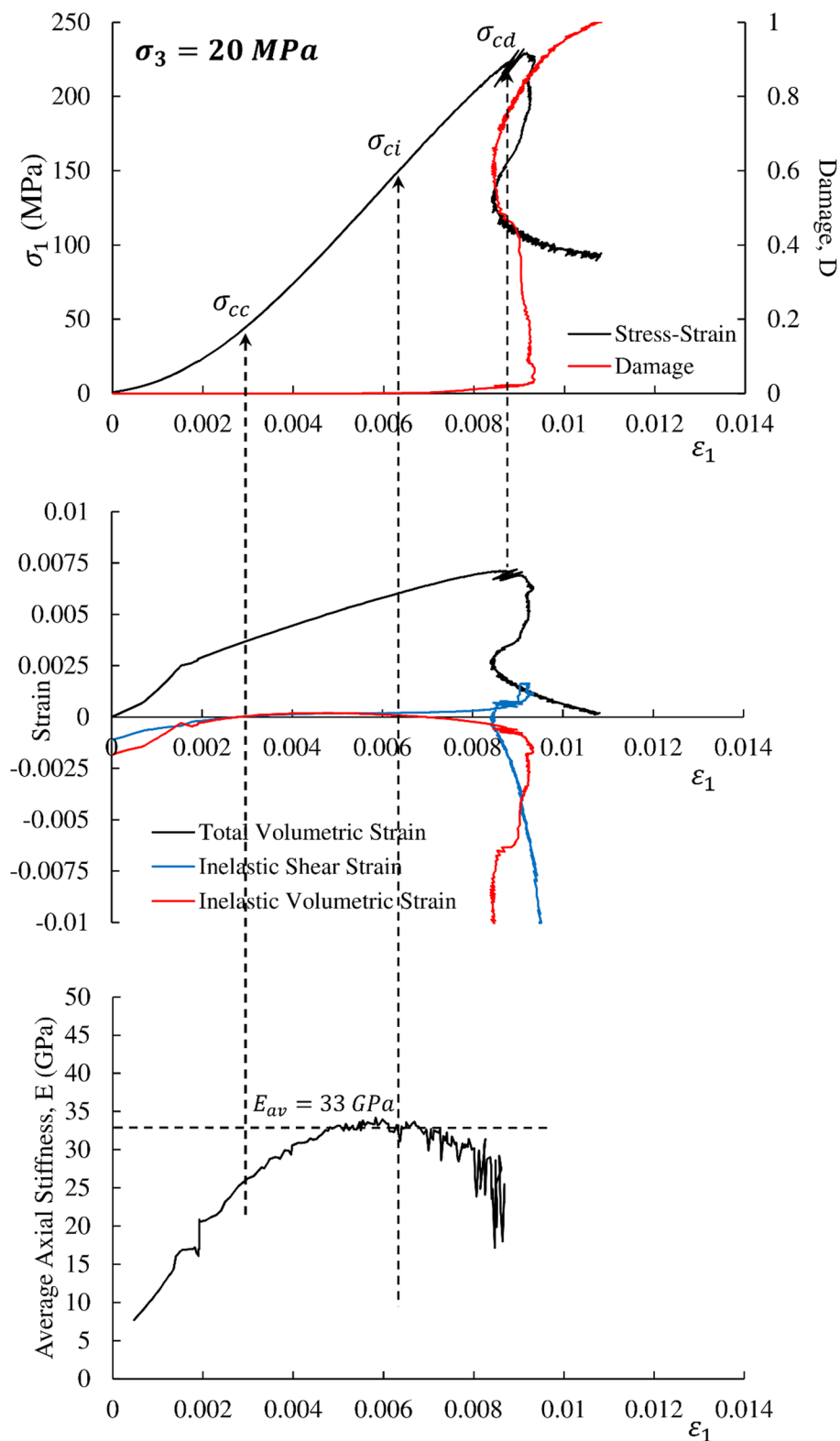
Fig. 14 Typical full test results for 10 MPa confinement



control (Table 1). When the volumetric strain reaches its peak value for each test the damage threshold is found to be 95–98% of the peak stress. This is also consistent when using the acoustic emission method. This highlights the

importance of the loading method in determining the point at which damage is uncontrollable. Therefore, if the pre-peak loading method is axial control, the crack damage threshold would be a lower percentage of the peak stress

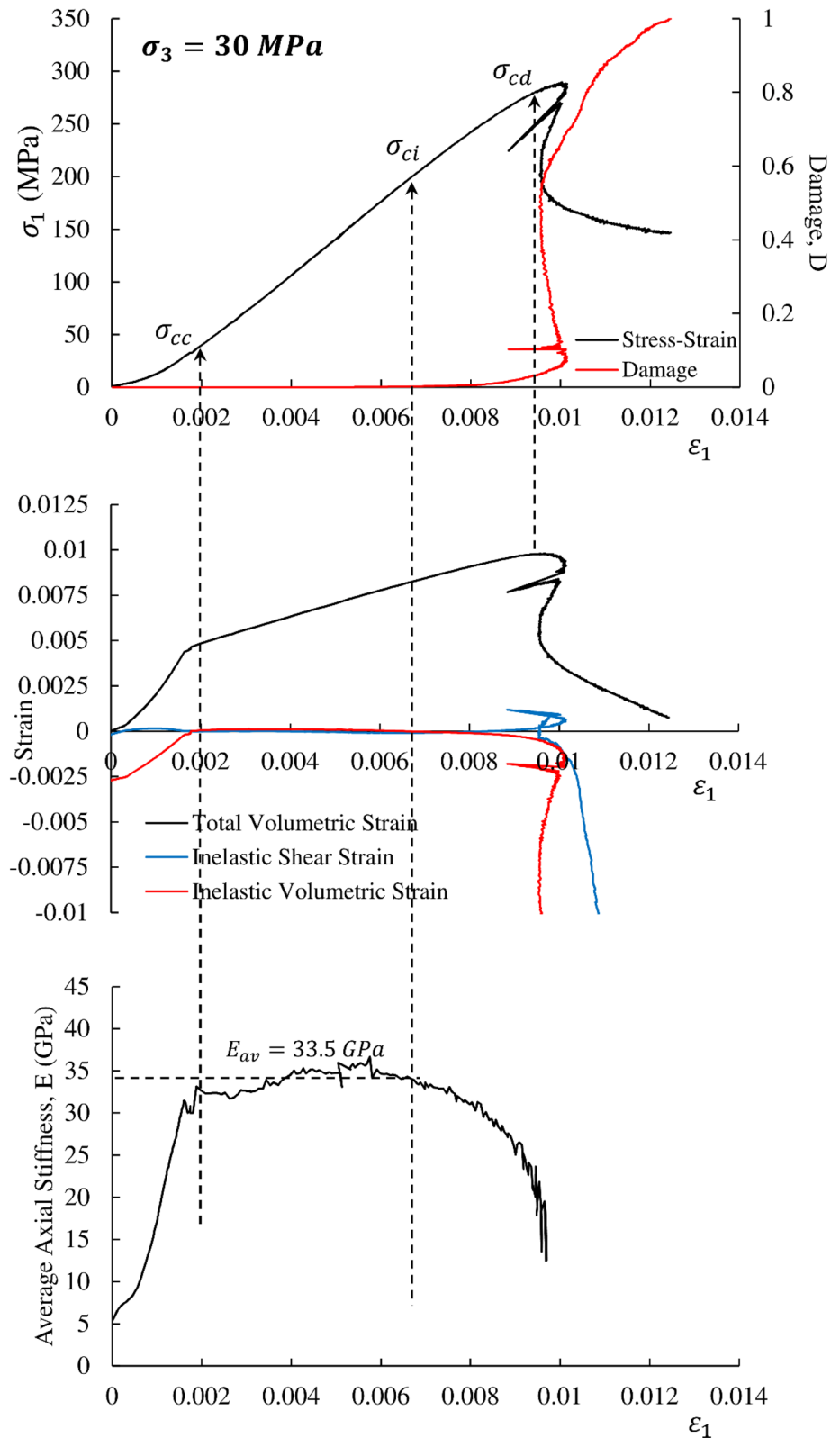
Fig. 15 Typical full test results for 20 MPa confinement



of a rock due to the constant application of displacement or load throughout the test. On the other hand, if the test is controlled by constant dilation of the specimen with time, which was implemented in the current research, the loading

can be relaxed and even reversed slightly to allow the rock to undergo self-sustaining failure where the post-peak response is not dependent on the stiffness of the loading frame. This has also been documented in other FCC studies

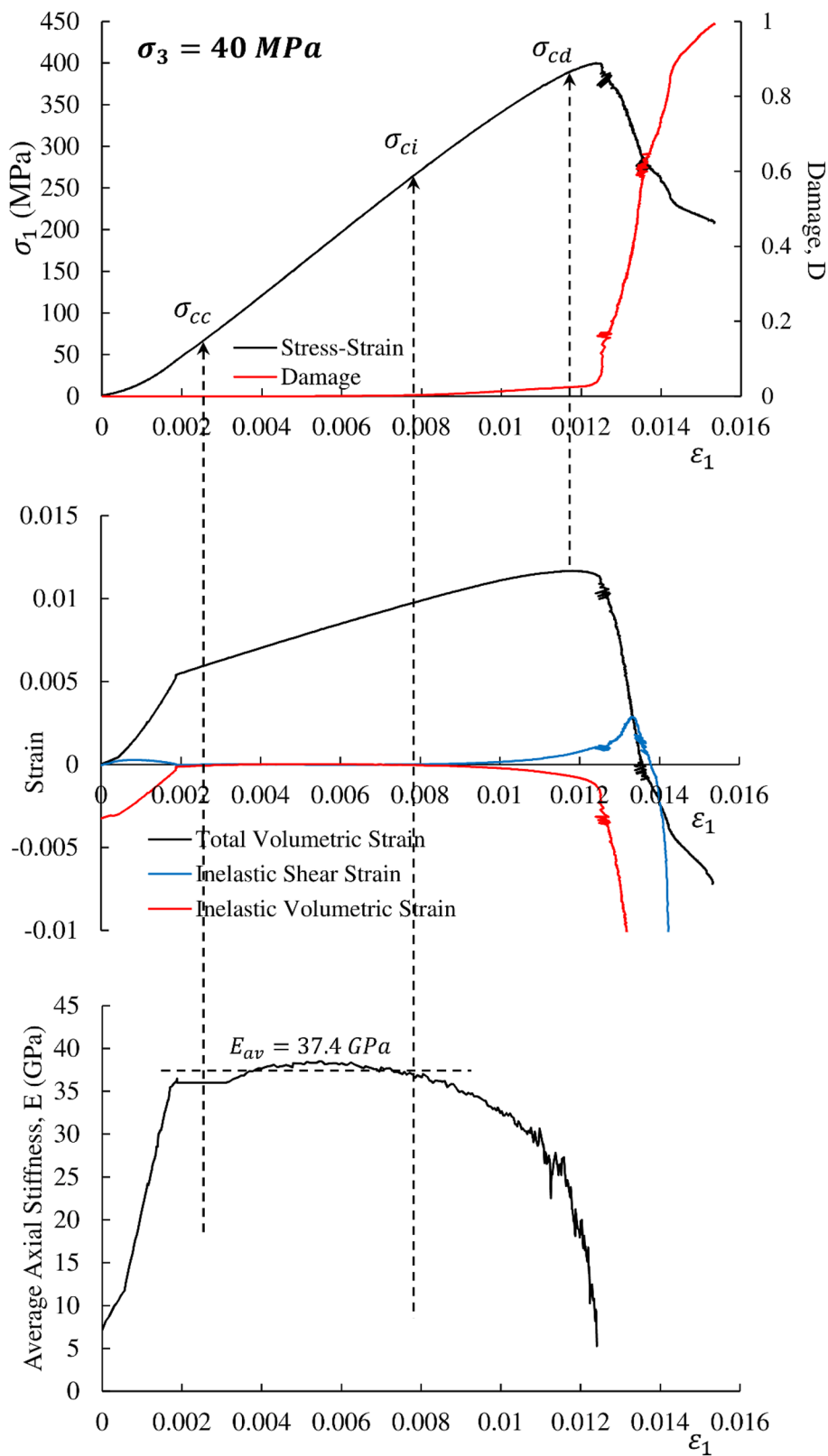
Fig. 16 Typical full test results for 30 MPa confinement



(Eloranta 2004; Jacobsson 2004a, b). Therefore, the damage is controllable up to much higher proportions of the peak stress. This is very important in the context of constitutive

modelling as the damage evolution is not loading rate or method dependent, allowing for accurate representation of material behaviour. Also, as the damage can be controlled

Fig. 17 Typical full test results for 40 MPa confinement



longer throughout the test, it provides much more accurate estimations of pre-peak damage levels in a material, which can then be used to effectively calibrate hardening and

softening phases in constitutive modelling. Other applications for this finding can be multiple-step triaxial loading or cyclic loading where the peak stress or damage level of the

Fig. 18 Typical full test results for 50 MPa confinement

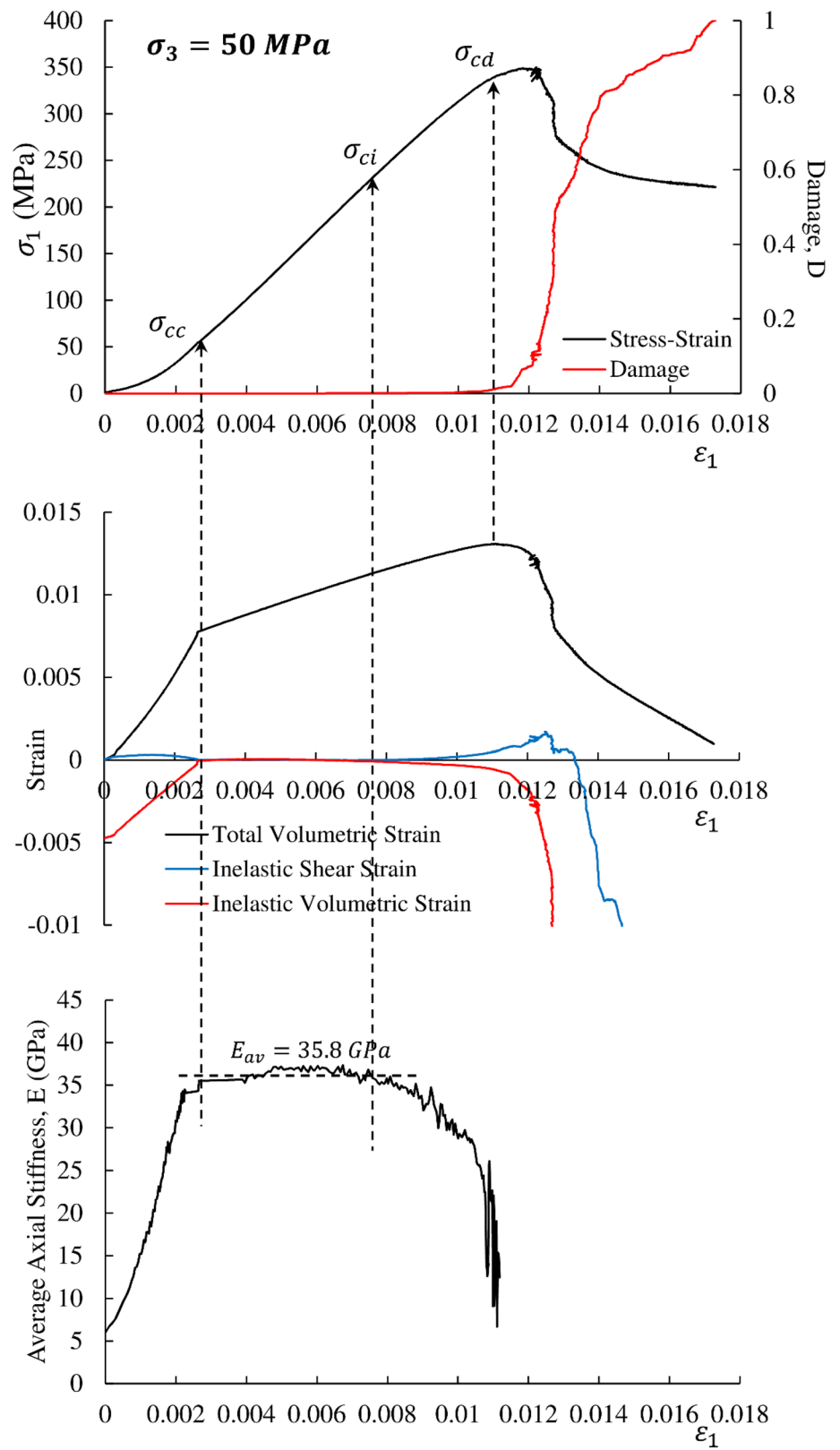


Fig. 19 Typical full test results for 60 MPa confinement

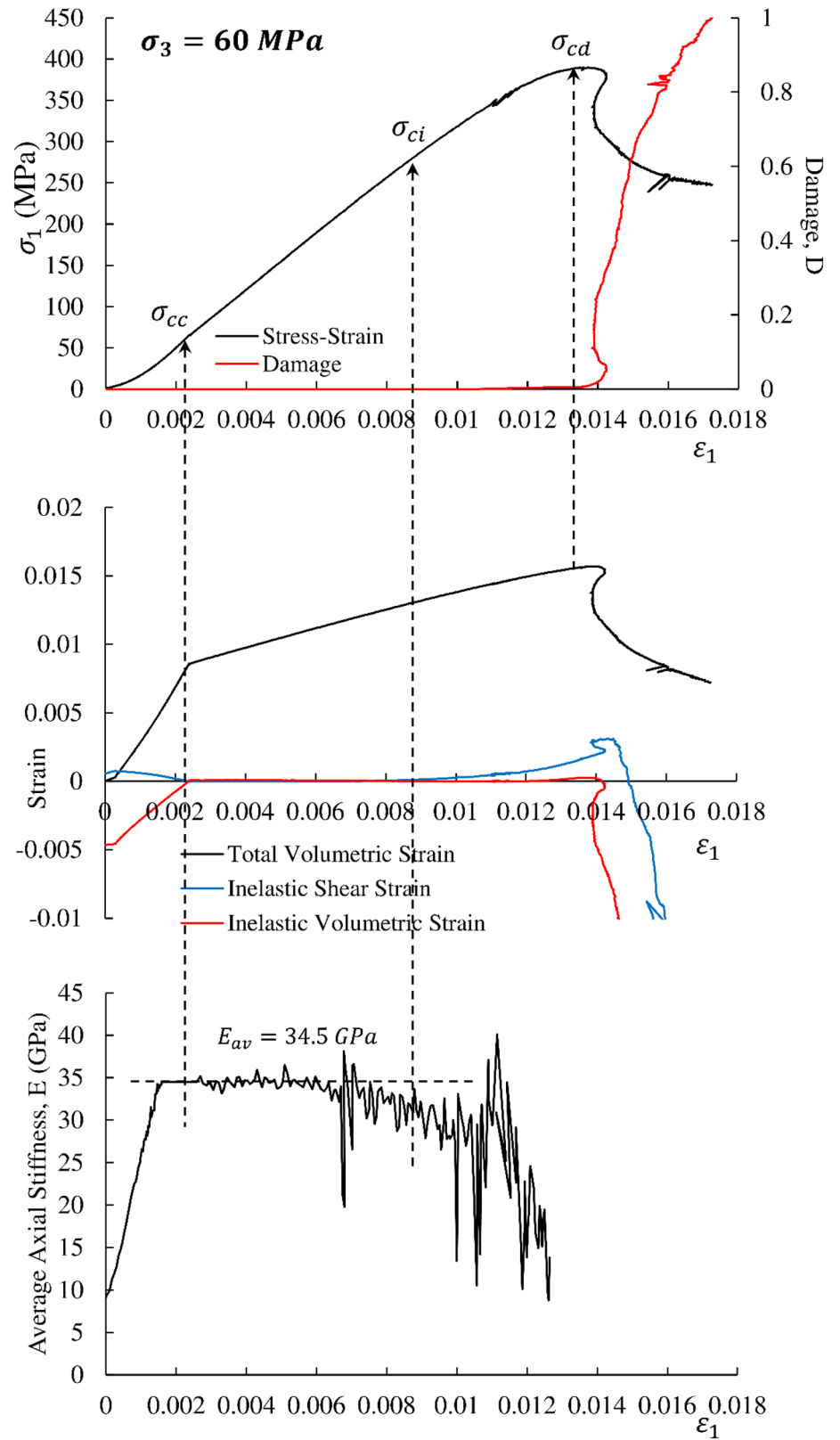


Table 3 Triaxial test results

| Sample ID | σ_3 (MPa) | σ_y (MPa) | σ_p (MPa) | σ_r (MPa) | E (GPa) | ν |
|-----------|------------------|------------------|------------------|------------------|-----------|-------|
| TX10-2 | 10 | 188.41 | 192.20 | 56.46 | 32.10 | 0.14 |
| TX10-3 | 10 | 184.09 | 186.33 | 71.53 | 33.70 | 0.14 |
| TX10-4 | 10 | 190.01 | 210.96 | 86.70 | 31.40 | 0.13 |
| TX10-5 | 10 | 155.33 | 167.98 | 65.02 | 35.10 | 0.14 |
| TX20-1 | 20 | 225.58 | 227.76 | 93.14 | 36.20 | 0.12 |
| TX20-2 | 20 | 248.57 | 269.24 | 162.27 | 36.70 | 0.14 |
| TX20-3 | 20 | 231.95 | 234.14 | 86.07 | 34.50 | 0.14 |
| TX20-5 | 20 | 292.18 | 306.79 | – | 33.50 | 0.13 |
| TX30-1 | 30 | 277.90 | 286.61 | 136.41 | 31.50 | 0.14 |
| TX30-2 | 30 | 225.36 | 232.63 | 126.49 | 31.60 | 0.14 |
| TX30-4 | 30 | 289.89 | 307.37 | 190.10 | 36.20 | 0.13 |
| TX40-1 | 40 | 364.18 | 391.86 | 201.76 | 37.40 | 0.12 |
| TX40-2 | 40 | 261.61 | 274.73 | 153.03 | 35.10 | 0.13 |
| TX40-3 | 40 | 364.18 | 375.84 | 218.51 | 36.50 | 0.11 |
| TX40-4 | 40 | 337.64 | 359.47 | 192.83 | 36.20 | 0.14 |
| TX50-1 | 50 | 326.00 | 343.46 | 216.12 | 35.80 | 0.14 |
| TX50-2 | 50 | 304.75 | 328.08 | 240.59 | 37.10 | 0.14 |
| TX50-3 | 50 | 372.61 | 393.59 | 257.57 | 36.70 | 0.15 |
| TX60-1 | 60 | 479.80 | 521.97 | 252.26 | 38.50 | 0.14 |
| TX60-2 | 60 | 350.12 | 388.05 | 231.95 | 34.40 | 0.14 |
| TX60-3 | 60 | 357.07 | 388.40 | 266.71 | 36.10 | 0.12 |

Table 4 Crack damage thresholds for each specimen

| Sample ID | σ_3 | σ_p | Crack initiation stress σ_{ci} (MPa) | | | | | | SD (MPa) | CoV | σ_{ci}/σ_p | Average σ_{ci}/σ_p | SD | CoV |
|-----------|------------|------------|---|-----|------|------|------|---------|----------|-------|------------------------|--------------------------------|------|-------|
| | | | ASM | LSR | CAEM | AEDM | DISM | Average | | | | | | |
| TX10-2 | 10 | 194 | 143 | 142 | 135 | 129 | 143 | 137 | 6.6 | 4.8% | 0.71 | 0.62 | 0.06 | 10.2% |
| TX10-3 | 10 | 186 | 110 | 105 | 96 | 100 | 117 | 105 | 9.1 | 8.7% | 0.56 | | | |
| TX10-4 | 10 | 211 | 130 | 129 | 121 | 131 | 120 | 125 | 5.6 | 4.4% | 0.59 | | | |
| TX10-5 | 10 | 168 | 101 | 96 | 110 | 95 | 107 | 102 | 7.6 | 7.5% | 0.61 | | | |
| TX20-1 | 20 | 236 | 168 | 151 | 136 | 152 | 146 | 146 | 7.3 | 5.0% | 0.62 | 0.68 | 0.06 | 9.0% |
| TX20-3 | 20 | 236 | 170 | 172 | 150 | 158 | 170 | 163 | 10.4 | 6.4% | 0.69 | | | |
| TX20-5 | 20 | 305 | 228 | 239 | 220 | 220 | 226 | 226 | 9.0 | 4.0% | 0.74 | | | |
| TX30-1 | 30 | 290 | 201 | 199 | 200 | 185 | 190 | 194 | 7.2 | 3.7% | 0.67 | 0.68 | 0.01 | 1.5% |
| TX30-2 | 30 | 234 | 178 | 133 | 163 | 178 | 163 | 159 | 18.9 | 11.9% | 0.68 | | | |
| TX30-4 | 30 | 308 | 215 | 220 | 210 | 208 | 208 | 212 | 5.7 | 2.7% | 0.69 | | | |
| TX40-1 | 40 | 400 | 260 | 295 | 250 | 280 | 293 | 280 | 20.8 | 7.4% | 0.70 | 0.71 | 0.02 | 2.6% |
| TX40-2 | 40 | 274 | 195 | 186 | 180 | 200 | 195 | 190 | 9.0 | 4.7% | 0.69 | | | |
| TX40-3 | 40 | 382 | 290 | 265 | 270 | 258 | 290 | 271 | 13.7 | 5.1% | 0.71 | | | |
| TX40-4 | 40 | 364 | 255 | 270 | 250 | 283 | 268 | 268 | 13.6 | 5.1% | 0.74 | | | |
| TX50-1 | 50 | 355 | 230 | 242 | 240 | 227 | 241 | 238 | 7.0 | 3.0% | 0.67 | 0.69 | 0.02 | 2.4% |
| TX50-2 | 50 | 329 | 220 | 210 | 233 | 243 | 235 | 230 | 14.2 | 6.2% | 0.70 | | | |
| TX50-3 | 50 | 394 | 280 | 277 | 277 | 261 | 282 | 274 | 9.1 | 3.3% | 0.70 | | | |
| TX60-1 | 60 | 522 | 387 | 391 | 388 | 403 | 380 | 391 | 9.5 | 2.4% | 0.75 | 0.72 | 0.07 | 9.3% |
| TX60-2 | 60 | 390 | 270 | 293 | 317 | 305 | 281 | 299 | 15.5 | 5.2% | 0.77 | | | |
| TX60-3 | 60 | 390 | 235 | 251 | 250 | 241 | 260 | 251 | 7.8 | 3.1% | 0.64 | | | |

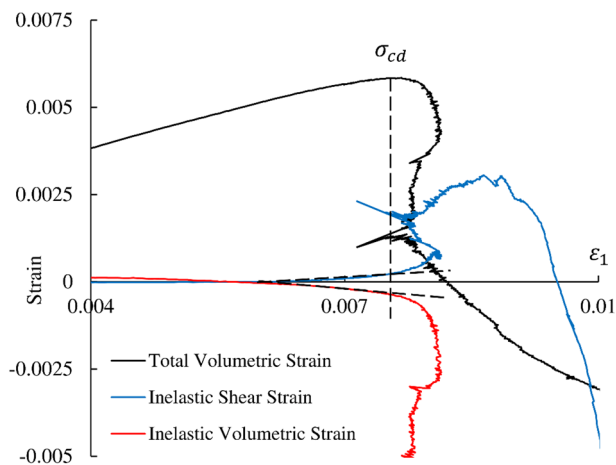


Fig. 20 Prediction of crack damage threshold with inelastic strain measures

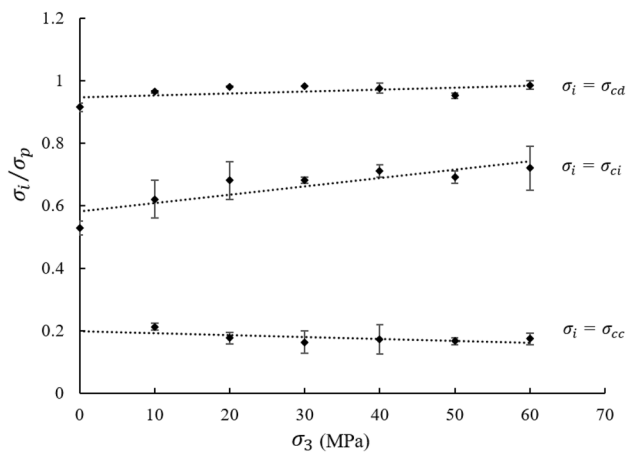


Fig. 21 Proportion of peak stress for each threshold over increasing confinement

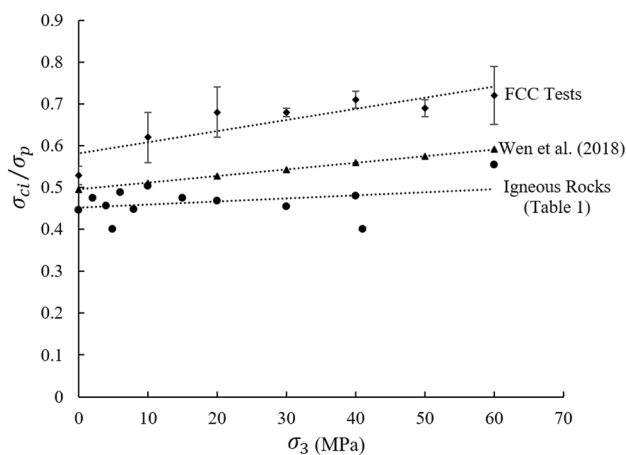


Fig. 22 Proportional crack initiation thresholds for FCC tests versus the literature data

specimen must be controlled and monitored throughout the duration of the test.

This study also shows that the circumferential strain method of control during a triaxial compression test can capture the range of Class I and II behaviours of a rock under the confining stress. It was found throughout most confinements that although the occurrence and degree of Class II behaviour was reduced with increased lateral pressure, it was still present and may not be lost until very high pressures are tested. This reveals that for engineering situations, such as the confinement levels addressed here, it is very important to obtain the ‘true’ stress–strain response of a material along with the associated damage evolution under these conditions. The experimental results also showed the transition phase of a material (in this case 40 MPa confinement), where the predominant response switches from Class II to I.

Finally, the relationship between damage evolution and confinement showed that as lateral stress increases, the rate of damage accumulation decreases. Due to the careful control method employed in this study, this response can be used in determining the effect of confinement on damage evolution and is again important to allow for correct modelling in damage–plasticity frameworks.

6 Conclusion

In this study, a series of triaxial compression tests were conducted using full circumferential strain control (FCC) on Class II rocks. The results were then used to identify damage thresholds using a variety of existing and proposed methods. It was found that although the crack closure threshold was similar to the literature, the crack initiation and damage thresholds were noticeably higher using this control method. The derived crack initiation thresholds identified that they are highly dependent on confining pressure, where the proportion of stress increases with increasing confinement. This indicates that contrary to some opinions, the damage thresholds are dependent on the method of test control and loading, more specifically on the stress–strain behaviour of Class I or II rocks. As the rock specimens in this paper were controlled by allowing self-sustaining dilation or failure, a more reliable estimation of crack initiation could be obtained. Therefore, values for the crack initiation thresholds found in this research can be directly applied as the ‘initial yield’ point in plasticity or damage–plasticity models as they provide more insight into material behaviour.

Another result of dilation control is that the crack damage threshold can be delayed until essentially the peak stress is obtained. Therefore, triaxial tests can be controlled for a lot longer with the circumferential method than for the axial control methods. The main advantage of this testing methodology is that the true pre- and post-peak

behaviours of a highly brittle rock can be captured alongside the true damage evolution under self-sustaining failure. This, in turn, is essential to correct modelling of engineering excavations using plasticity or damage-plasticity frameworks as it provides a more complete and justifiable dataset for the rock tested.

Acknowledgements This research team would like to gratefully acknowledge the Australian Research Council (LP150100539) and OZ Minerals Ltd for their ongoing financial and technical support for this project. The team would also like to gratefully acknowledge the laboratory staff, in particular Adam Ryntjes and Simon Golding.

References

- Akdag S, Karakus M, Taheri A, Nguyen G, He M (2018) Effects of thermal damage on strain burst mechanism for brittle rocks under true-triaxial loading conditions. *Rock Mech Rock Eng*. <https://doi.org/10.1007/s00603-018-1415-3>
- Bieniawski Z (1967a) Mechanism of brittle fracture of rock: part I—theory of the fracture process. *Int J Rock Mech Min Sci* 4:395–406
- Bieniawski Z (1967b) Mechanism of brittle fracture of rock: part II—experimental studies. *Int J Rock Mech Min Sci* 4:407–423
- Bruning T, Karakus M, Nguyen G, Goodchild D (2016) Development of a unified yield-failure criterion for the modelling of hard rocks. In: *International Conference on Geomechanics, Geo-energy and Geo-resources (IC3G)*, Melbourne, Australia
- Butt S, Mukherjee C, Lebars G (2000) Evaluation of acoustic attenuation as an indicator of roof stability in advancing headings. *Int J Rock Mech Min Sci* 37:1123–1131
- Chang S, Lee C (2004) Estimation of cracking and damage mechanisms in rock under triaxial compression by moment tensor analysis of acoustic emission. *Int J Rock Mech Min Sci* 41:1069–1086
- Chen L, Liu J, Wang C, Liu J, Su R, Wang J (2014) Characterisation of damage evolution in granite under compressive stress condition and its effect on permeability. *Int J Rock Mech Min Sci* 71:340–349
- Chen L, Wang C, Liu J, Liu J, Wang J, Jia Y, Shao J (2015) Damage and plastic deformation modeling of Beishan granite under compressive stress conditions. *Rock Mech Rock Eng* 48:1623–1633
- Cox S, Meredith P (1993) Microcrack formation and material softening in rock measured by monitoring acoustic emissions. *Int J Rock Mech Min Sci* 30:11–24
- Eberhardt E, Stead D, Stimpson B, Read R (1998) Identifying crack initiation and propagation thresholds in brittle rock. *Can Geotech J* 35:222–233
- Eberhardt E, Stead D, Stimpson B (1999) Quantifying progressive pre-peak brittle fracture damage in rock during uniaxial compression. *Int J Rock Mech Min Sci* 36:361–380
- Eloranta P (2004) Forsmark site investigation, Drill hole KFM01A, Triaxial compression test (HUT), P-04-177. Helsinki University of Technology, Rock Engineering, Stockholm
- Fairhurst C, Hudson J (1999) Draft ISRM suggested method for the complete stress-strain curve for intact rock in uniaxial compression. *Int J Rock Mech Min Sci* 36:279–289
- Fonseka G, Murrell S, Barnes P (1985) Scanning electron microscope and acoustic emission studies of crack development in rocks. *Int J Rock Mech Min Sci Geomech Abstr* 22:273–289
- Fredrich J, Wong T (1986) Micromechanics of thermally induced cracking in three crustal rocks. *J Geophys Res* 91:12743–12764
- Ghazvinian E, Diederichs M, Labrie D, Martin C (2015) An investigation on the fabric type dependency of the crack damage thresholds in brittle rocks. *Geotech Geol Eng* 33:1409–1429
- Grosse C, Ohtsu M (2008) *Acoustic emission testing*. Springer, Germany
- Hatzor Y, Palchik V (1997) The influence of grain size and porosity on crack initiation stress and critical flaw length in dolomites. *Int J Rock Mech Min Sci* 34:805–816
- Heo J, Cho H, Lee C (2001) Measurement of acoustic emission and source location considering anisotropy of rock under triaxial compression. In: Sarkka P, Eloranta P (eds) *Rock mechanics—a challenge for society*. Swets & Zeitlinger Lisse, Espoo, pp 91–96
- Hidalgo K, Nordlund E (2013) Comparison between stress and strain quantities of the failure-deformation process of fennoscandian hard rocks using geological information. *Rock Mech Rock Eng* 46:41–51
- Hoek E, Martin C (2014) Fracture initiation and propagation in intact rock—a review. *J Rock Mech Geotech Eng* 6:287–300
- Hudson J, Brown E, Fairhurst C (1970) Shape of the complete stress-strain curve for rock. Paper presented at the Proc. 13th symp. on Rock Mech., University of Illinois
- Hudson J, Crouch S, Fairhurst C (1972) Soft, stiff and servo-controlled testing machines: a review with reference to rock failure. *Eng Geol* 6:155–189
- ISRM (2007) *The complete ISRM suggested methods for rock characterization, testing and monitoring: 1974–2006*. Ulusay R, Hudson JA (eds) Prepared by the commission on testing methods. ISRM, Ankara
- Jacobsson L (2004a) Forsmark site investigation, Borehole KFM01A, Triaxial compression test of intact rock, P-04-227. SP Swedish National Testing and Research Institute, Stockholm
- Jacobsson L (2004b) Oskarshamn site investigation, Borehole KLX04A, Triaxial compression test of intact rock, P-04-262. SP Swedish National Testing and Research Institute, Stockholm
- Ji M, Zhang Y, Liu W, Cheng L (2014) Damage evolution law based on acoustic emission and Weibull distribution of granite under uniaxial stress. *Acta Geodyn Geomater* 11:269–277
- Katz O, Reches Z (2004) Microfracturing, damage and failure of brittle granites. *J Geophys Res* 109:B01206
- Kim J, Lee K, Cho W, Choi H, Cho G (2015) A comparative evaluation of stress-strain and acoustic emission methods for quantitative damage assessments of brittle rock. *Rock Mech Rock Eng* 48:495–508
- Krajcinovic D (1996) *Damage mechanics*. North-Holland, Amsterdam
- Labuz J, Bialzi L (1991) Class I vs Class II stability: a demonstration of size effect. *Int J Rock Mech Min Sci Geomech Abstr* 28:199–205
- Lemaitre J, Desmorat R (2005) *Engineering damage mechanics*. Springer-Verlag, Berlin
- Lockner D (1993) The role of acoustic emission in the study of rock fracture. *Int J Rock Mech Min Sci Geomech Abstr* 30:883–899
- Ma T, Tang C, Tang L, Zhang W, Wang L (2015) Rockburst characteristics and microseismic monitoring of deep-buried tunnels for Jinping II hydropower station. *Tunn Undergr Sp Tech* 49:345–368
- Martin C (1993) The strength of massive Lac du Bonnet granite around underground openings. PhD Thesis, University of Manitoba, USA
- Martin C, Chandler N (1994) The progressive fracture of Lac du Bonnet granite. *Int J Rock Mech Min Sci Geomech Abstr* 31:643–659
- Murakami S (2012) *Continuum damage mechanics*. Springer, London
- Nicksiar M, Martin C (2012) Evaluation of methods for determining crack initiation in compression tests on low-porosity rocks. *Rock Mech Rock Eng* 45:607–617
- Oda M, Takemura T, Aoki T (2002) Damage growth and permeability change in triaxial compression tests of Inada granite. *Mech Mater* 34:313–331
- Puzrin A (2012) *Constitutive modelling in geomechanics*. Springer-Verlag, Berlin

- Salari M, Saeb S, William K, Pachet S, Carrasco R (2004) A coupled elastoplastic damage model for geomaterials. *Comput Methods Appl Mech Eng* 193:2625–2643
- Tang C, Wang J, Zhang J (2010) Preliminary engineering application of microseismic monitoring technique to rockburst prediction in tunneling of Jinping II project. *Chin J Rock Mech Eng* 2:193–208
- Tapponnier P, Brace W (1976) Development of stress-induced microcracks in Westerly granite. *Int J Rock Mech Min Sci Geomech Abstr* 13:103–112
- Unteregger D, Fuchs B, Hofstetter G (2015) A damage plasticity model for different types of intact rock. *Int J Rock Mech Min Sci* 80:402–411
- Wawersik W (1968) Detailed analysis of rock failure in laboratory compression tests. PhD Thesis University of Minnesota, USA
- Wawersik W, Brace W (1971) Post-failure behavior of a granite and diabase. *Rock Mech* 3:61–85
- Wawersik W, Fairhurst C (1970) A study of brittle rock fracture in laboratory compression experiments. *Int J Rock Mech Min Sci* 7:561–575
- Wen T, Tang H, Ma J, Wang Y (2018) Evaluation of methods for determining crack initiation stress under compression. *Eng Geol* 235:81–97
- Wong T (1982) Micromechanics of faulting in Westerly granite. *Int J Rock Mech Min Sci Geomech Abstr* 19:19–49
- Zhang Z, Zhang R, Xie H, Liu J, Were P (2015) Differences in the acoustic emission characteristics of rock salt compared with granite and marble during the damage evolution process. *Environ Earth Sci* 73:6987–6999
- Zhao X, Cai M, Wang J, Ma L (2013) Damage and acoustic emission characteristics of the Beishan granite. *Int J Rock Mech Min Sci* 64:258–269
- Zhao X, Cai M, Wang J, Li P, Ma L (2015) Objective determination of crack initiation stress of brittle rocks under compression using AE measurement. *Rock Mech Rock Eng* 48:2473–2484
- Zong Y, Han L, Wei J, Wen S (2016) Mechanical and damage evolution properties of sandstone under triaxial compression. *Int J Min Sci Technol*. <https://doi.org/10.1016/j.ijmst.2016.05.011> (in press)

Publisher's Note Springer Nature remains neutral with regard to jurisdictional claims in published maps and institutional affiliations.